ELSEVIER

S0032-3861(96)00188-7

Polymer Vol. 37 No. 16, pp. 3623–3636, 1996

0032-3861/96/$15.00 + 0.00

Crystallization behaviour of poly(*p*-phenylene sulfide): effects of molecular weight fractionation and endgroup counter-ion

Brian G. Risch, Srivatsan Srinivas and Garth L. Wilkes*
Polymer Materials and Interfaces Laboratory, Virginia Polytechnic Institute and State University, Blacksburg, VA 24061, USA

and Jon F. Geibel, Carlton Ash†, Scott White‡ and Michael Hicks
Phillips Petroleum Company, Bartlesville, OK 74004, USA
(Received 10 September 1995; accepted 1 February 1996)

The crystallization behaviour of poly(*p*-phenylene sulfide) (PPS) has been studied. Two PPS samples with $\langle M_w \rangle = 44\,K$ and $\langle M_w \rangle = 64\,K$ were fractionated by a process which selectively removes a portion of the low molecular weight species yielding fractionated PPS samples with $\langle M_w \rangle = 56\,K$ and $\langle M_w \rangle = 104\,K$ respectively. The fractionated samples were then treated with an ion exchange process to allow control over the nature of endgroup counter-ion, i.e. to introduce Na^+ and Zn^{2+} ions. Using a Hoffman–Weeks analysis, the equilibrium melting temperature of these polymers was estimated to be 320°C irrespective of endgroup counter-ion or polymer molecular weight. The nucleation density was observed to increase as a function of molecular weight by small-angle light scattering (SALS). The spherulitic growth rates and nucleation densities were studied as a function of the chemical nature of endgroup counter-ion for PPS with $\langle M_w \rangle = 56\,K$ that had been fractionated to remove low molecular weight species. Additionally, isothermal rates of bulk crystallization were analysed as a function of molecular weight of PPS and chemical nature of the endgroup counter-ion. It was found that as a function of endgroup counter-ion, crystal growth rates and overall crystallization rates decreased in the following order: $H^+ > Zn^{2+} > Na^+$. The order of decreasing crystal growth rates corresponded to a similar increase in melt viscosity as a function of endgroup counter-ion, suggesting that the reason for decreasing growth rates could originate from increasing secondary interchain interactions. Optical microscopy studies showed the nucleation density decreased in the order $H^+ > Na^+$. The ion-exchange reactions were shown to be reversible by differential scanning calorimetry (d.s.c.) and optical microscopy studies. Crystallinity determinations by wide angle X-ray diffraction (WAXD) and measurements of the heats of melting illustrated that higher molecular weight PPS attained lower levels of crystallinity than PPS of lower molecular weight when crystallized under identical conditions.

(Keywords: PPS; crystallization; endgroups)

INTRODUCTION

Poly(*p*-phenylene sulfide) (PPS) is a high temperature semicrystalline thermoplastic polymer that combines the properties of excellent chemical resistance, flame resistance, and mechanical strength[1–3]. PPS is known to undergo curing reactions which increase its molecular weight, toughness, ductility and solvent resistance[4]. Due to this overall combination of properties, PPS is finding increased use as a moulding resin and has also been used as a matrix material for thermoplastic composites. Additional specific applications include pump impellers, ball valves, wear rings, electrical sockets, as well as battery and telephone components[5,6]. PPS may also be made conductive by the addition of dopants[7–9].

The properties of semicrystalline polymers such as PPS depend on the extent of crystallinity and morphological superstructure of the polymer. Numerous studies have been undertaken to investigate the crystalline structure, morphology, thermal stability, and crystallization kinetics of PPS. Jog and coworkers studied the isothermal crystallization of PPS, and using a classical Avrami analysis, found an Avrami exponent between 2.0 and 2.2[10,11]. Lovinger *et al.* studied the spherulitic growth rates of PPS with $\langle M_w \rangle = 15\,000$ and $\langle M_w \rangle = 51\,000$ and found a maximum in the spherulitic growth rate of PPS at 180°C[12] utilizing unfractionated PPS. López *et al.* studied the effects of molecular weight, branching, and endgroup counter-ion on the crystallization behaviour of PPS[13–16]. The crystal growth rates were found to decrease as molecular weight increased

* To whom correspondence should be addressed
† Present address: Shell Research Center, Houston, TX
‡ Present address: Becton Dickinson Research Center, Research Triangle Park, NC, USA

Table 1 Summary of possible endgroup chemistry for PPS

Endgroup	Expected?	Observed?	Comment	Reference
Chlorophenyl	Yes	Yes		18, 19
Thiophenoxide	Yes	No		18
Amines	No	Yes	On oligomer	18
Butanoate	No	Speculated	Expected from amine	17, 18
Phenylthio	No	Yes	On polymer	18
			On oligomer	19
Phenyloxy	No	Yes	On oligomer	19
Phenoxide	No	Speculated	Required intermediate	19

while the nucleation density increased as molecular weight increased. Increasing branch content through the incorporation of a comonomer, 1,2,4-trichlorobenzene was found to reduce both the crystalline growth rate as well as nucleation density[15].

The identification of chain endgroups, and particularly ionizable endgroups, on PPS is of considerable importance in view of their possible effects on crystallization behaviour. However, as will be discussed later, very few publications describe unambiguous identifications of PPS endgroup chemistry due to analytical difficulties in characterizing low concentrations of these species in PPS polymers. It has been demonstrated that the effect of ion-exchange reactions on PPS is to alter the crystallization behaviour, evidenced by changes in spherulitic growth rates and nucleation densities observed by López *et al.*[13–15].

The polymerization used to produce linear PPS as practiced by Phillips Petroleum Company and described by Fahey and Ash[17] is a series of nucleophilic displacement reactions of hydrosulfide initially, and aryl mercaptides later in the polymerization, with aryl chlorides. The polymerization is carried out with a slight excess of aryl chloride species to avoid conditions leading to polymer degradation. As such, one would expect that the sulfur nucleophiles are the limiting reagent and, in principle, should be consumed during the course of the polymerization. This leads to the expectation that residual aryl chlorides will comprise PPS endgroups. Indeed, aryl chloride endgroups have been observed in high temperature n.m.r. studies of PPS by Wade *et al.*[18] and in mass spectral studies of oligomers extracted from PPS by Reents and Kaplan[19]. Aryl mercaptide endgroups, expected only for PPS polymerizations not run to completion, were not observed in labelled endgroup derivatization studies by Wade *et al.*[18]. However, this finding was rationalized on the basis that the conditions used to derivatize the nucleophilic mercaptide endgroups were shown to be ineffective when attempting to derivatize a model compound, thiophenol.

One surprising finding by Wade *et al.*, was that of nitrogen containing endgroups. Both substituted and unsubstituted amine endgroups were detected on PPS. The only source of nitrogen compounds in the PPS samples studied was from the solvent used for polymerization, N-methyl-2-pyrrolidone (NMP). A reasonable hypothesis for the existence of nitrogen-containing endgroups on PPS is nucleophilic attack of the nitrogen moiety in sodium N-methyl-4-aminobutanoate (SMAB), a known intermediate[17] in PPS polymerizations. The fact that the nitrogen from SMAB may function as a nucleophile to displace chloride ions from aryl chloride endgroups may lead to nitrogen containing endgroups. It is also worth noting that this side reaction may also result in covalent attachment of carboxylic acid endgroups on PPS. Such carboxylic acids would certainly be expected to participate in the ion-exchange reactions. Unsubstituted amine endgroups may result from the decomposition of the 4-aminobutanoate moiety. Additional protonation/deprotonation may involve the anilines produced in the side reactions.

Other endgroups were identified by Reents and Kaplan such as 4-chlorophenyloxy- and phenyloxy-endgroups. The formation of these endgroups is predicated on the reaction of a phenoxide nucleophile with either monomer (*p*-dichlorobenzene) or aryl chloride polymer endgroups. Phenoxide nucleophiles are most probably a result of hydrolysis of aryl chloride species under the highly basic PPS polymerization conditions. Since aryl chloride endgroups are known for PPS, it is, therefore, reasonable to hypothesize the presence of phenoxide endgroups. Since phenols have acid dissociation constants around 10, it is reasonable to expect that this type of endgroup would also be responsive to protonation/deprotonation reactions as well as cation exchange reactions.

Unsubstituted phenyl endgroups were detected by Reents and Kaplan both as phenylthio- and phenyloxy-endgroups. Presumably, these endgroups result from reductive dehalogenation of aryl chloride endgroups. Although not proven to occur under PPS reaction conditions, such dehalogenation can be accomplished by the single electron transfer mechanism postulated by Novi *et al.*[20]. Such a mechanism has recently been suggested by Percec *et al.*[21] for reductive halogenations occurring during polyetherification of bis(aryl chloride)s by hydroquinone nucleophiles. A key intermediate in the single electron transfer mechanism is a phenyl radical, which may abstract a hydrogen from the solvent (NMP), thereby producing an unsubstituted phenyl endgroup. Although the mechanism is speculative, the existence of such endgroups is clear. Equally clear is that such unsubstituted endgroups are unable to participate in either protonation/deprotonation or ion exchange reactions. A summary of the possible endgroups for PPS is presented in *Table 1*.

Due to the different possible mechanisms for termination of the polymerization of PPS, many endgroup species are present, some of which may possess an ionic character. In earlier work by López *et al.* on PPS samples which had undergone an effective ion-exchange process

to control the chemical nature of ionizable endgroups, the crystal growth rates were observed to decrease as a function of endgroup counter-ion in the following order: $Ca^{2+} > H^+ > Zn^{2+} > Na^+$. Nucleation densities were also found to decrease in the following order: $H^+ > Na^+ > Zn^{2+} > Ca^{2+}$ [13–15]. These observations will be reinforced by the results of our studies presented in this paper. *It should be noted here that the present study utilized fractionated polymers containing significantly fewer low molecular weight species as compared to the unfractionated polymers studied by López* et al. *in their earlier work.*

Several studies have been undertaken to investigate the effect of melt history on PPS. The melt history may have a profound influence on the crystallization rate of PPS since the melt hold temperature and residence time can affect both the number of surviving crystalline nuclei (commonly called residual nuclei) and the extent to which chain extension and crosslinking reactions occur. Menczel and Collins observed that upon successive heating of the melt to 350°C, crystallization of PPS was retarded[22,23], a result consistent with the earlier findings of Brady[24]. However, this melt temperature is well above necessary melt processing conditions typically employed. A more extensive study by Mehl and Rebenfeld on Fortron® PPS revealed that the crosslinking and chain extension reactions that occur at high temperatures significantly alter the rate of crystallization as well as the degree of crystallinity of PPS[25]. This trend was found to be highly accelerated at melt temperatures above 320°C, and lower molecular weight species were found to be more susceptible to chain extension and crosslinking reactions.

The present work investigates the effects of molecular weight fractionation and endgroup counter-ion on the nucleation density, crystalline growth rate, and bulk crystallization behaviour of PPS by differential scanning calorimetry (d.s.c.), polarized optical microscopy (POM), small angle light scattering (SALS), and wide angle X-ray diffraction (WAXD). This study was undertaken in order to examine the effects that possible ionic endgroup interactions have on the rheological properties and crystallization behaviour of PPS. By utilizing fractionated, ion-exchanged PPS, the results of this study may be compared to the results of an earlier study by López *et al.*[14] on unfractionated ion-exchanged samples, thus giving information about the effects of fractionation as well.

EXPERIMENTAL

Material

The linear poly(*p*-phenylene sulfide) samples used in this study were synthesized via the process developed by Campbell[26]. The characterization of weight average molecular weight and molecular weight distributions were obtained by means of a gel permeation chromatographic (g.p.c.) technique in α-chloronaphthalene at 220°C originally developed by Stacy[27]. In contrast to the viscometric detector used by Stacy, in this study a flame ionization detector (FID) was used to measure polymer which elutes from the column. Although improved over the viscometric detector, this type of detector has reduced sensitivity for species with molecular weights below 1000 g mol^{-1}, because in the process of solvent evaporation, the polymer passes through a heated region where some low molecular weight species may be volatilized. Since these low molecular weight species are most abundant in step-growth polymerizations, it would be expected that number average molecular weights obtained from such a detector may be artificially high. Therefore only weight average molecular weights are reported in this study.

Table 2 G.p.c. and rheological characterization of the samples used in this study

Sample designation	$\langle M_w \rangle$	(Poise, 1 rad s^{-1})[a]
Parent #1	64 000	13 100
Fraction #1	104 000	47 000
Acid wash of Fraction #1	96 000	43 000
Na^+ exchange of AW Fraction #1[b]	102 000	55 800
Zn^{2+} exchange of AW Fraction #1[b]	106 000	55 900
Parent #2	44 000	2 800
Fraction #2	56 000	5 200
Acid wash of Fraction #2	54 000	4 800
Na^+ exchange of AW Fraction #2[b]	57 000	5 300
Zn^{2+} exchange of AW Fraction #2[b]	60 000	5 500

[a] Data obtained at 300°C and 1 rad s^{-1}
[b] AW = acid washed

The 'Parent' samples were received 'as polymerized'. The high molecular weight parent sample (Parent #1—see *Table 2*) was recovered from the reaction mixture by a process[28] which gives this sample a slight fractionation of the low molecular weight oligomers, whereas the low molecular weight parent sample (Parent #2—see *Table 2*) was recovered by a technique[29] which removes essentially no oligomers at all. Therefore there is a more prominent 'hump' in the g.p.c. scans for Parent #2 and the respective fractions than in those for Parent #1 and the respective fractions—see *Figure 1*.

The respective parent samples were then further fractionated using a technique developed by Ash *et al.*[30] to remove additional low molecular weight oligomers. The parent polymers were dissolved in a mixture of NMP and distilled water and charged to a high pressure titanium autoclave equipped with a stirrer. The stirred reaction mixture was deoxygenated by pressurizing the autoclave with nitrogen to approximately 200 psig and then carefully releasing the pressure. Deoxygenation was effected by repeating the above pressurize-release procedure five times. The reaction mixture was then heated to either 260°C (Parent #1) or 265°C (Parent #2), after which the agitation was stopped. The reaction mixture separated into two liquid phases, a more dense polymer-rich phase containing essentially all of the high molecular weight polymer, and a portion of the lower molecular weight polymer and oligomers, and a less dense polymer-lean phase containing essentially no high molecular weight polymer and the remainder of the lower molecular weight polymer and oligomers. The polymer from the polymer-rich phase was collected and washed exhaustively with distilled water to remove residual NMP. The polymer was then dried at 100°C in a vacuum oven to a constant weight.

The specimens utilized to study the effects of endgroup counter-ion were prepared by using an effective ion-exchange procedure on powders of the fractionated specimens. In an earlier study by López *et al.*, the same ion-exchange procedure was performed on samples with $\langle M_w \rangle = 63$ K which had not been fractionated[14]. The

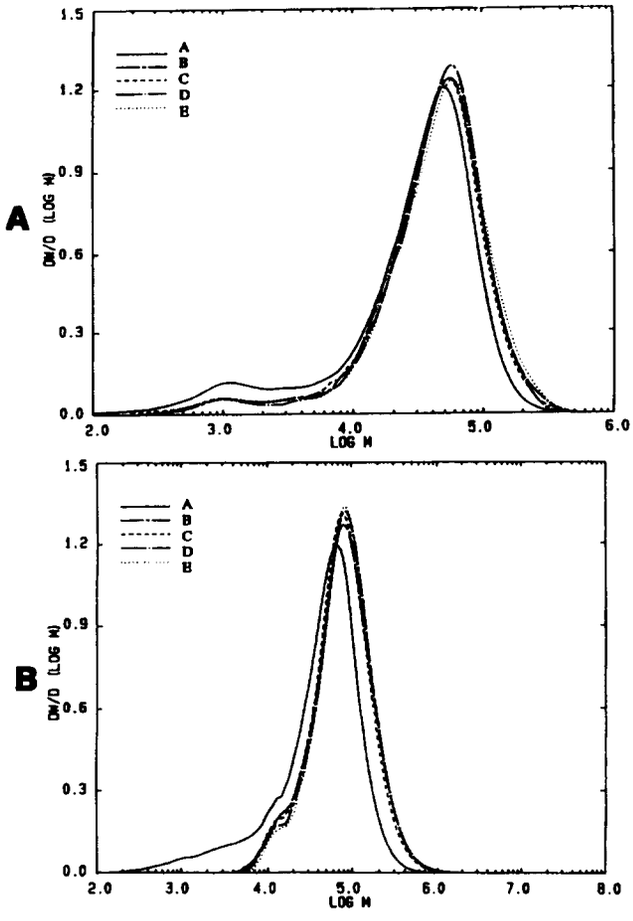

Figure 1 Molecular weight distributions obtained from g.p.c. experiments. (A) A, Parent #2; B, Fraction #2; C, Acid wash of Fraction #2; D, Na^+ wash of fraction #2; E, Zn^{2+} wash of Fraction #2. (B) A, Parent #1; B, Fraction #1; C, Acid wash of Fraction #1; D, Na^+ wash of Fraction #1; E, Zn^{2+} wash of Fraction #1

existing metal ions present in the polymer were first removed by charging the powdered solid PPS and a dilute solution of acetic acid (1% v:v) to a titanium autoclave. The reaction mixture was deoxygenated by pressurizing to 200 psig with nitrogen and then releasing the pressure. This pressurization/release cycle was repeated six times. Deoxygenating in this manner eliminates oxygen from the autoclave and minimizes the possibility of oxidative chain extension. The reaction mixture was then heated to 235°C with agitation for 1 h. The polymer slurry was then cooled, filtered and the recovered polymer was washed with glass distilled water at room temperature to remove any residual adsorbed acetic acid solution. A sample of the acid washed polymer was analysed for residual metal ions. To introduce specific metal ions to the acid-washed polymer, this polymer was again charged to the autoclave along with a dilute metal acetate solution (1% w:v). Deoxygenating was performed as described earlier. The reaction mixture was heated to 235°C for 30 min, cooled and recovered as described above. All samples were dried to a constant weight in a vacuum oven at 100°C prior to analysis. *Table 2* summarizes the samples used in this study. The apparent small increase in molecular weight as a function of endgroup counterion for the ion-exchanged species is likely the result of aggregation of some of the ionic endgroups in the α-chloronaphthalene solution during g.p.c. measurement.

To confirm that the ion-exchange process was reversible, some of the fractionated low molecular weight sample that had Na^+ endgroups ($\langle M_w \rangle$ = 57 000) was washed with acetic acid as described above to reintroduce acid endgroups. Subsequently, a portion of this sample was again subjected to an ion-exchange process as described above to reintroduce Na^+ ions. These samples will henceforth be referred to as Na1, Acid wash2, and Na2 in this paper.

Morphological experiments

PPS specimens were pressed into thin films between glass cover slips at 320°C prior to growth rate and morphological measurements. A Zeiss polarizing optical microscope equipped with a Linkam THM 600 heating stage and a 35 mm camera was used for polarized optical microscopy experiments. Due to the fact that melt treatment of PPS at high temperatures (especially above 320°C) for extended periods of time, may lead to thermally induced charges, samples were heated for 320°C for only 4 min prior to crystallization. The samples were then rapidly quenched to the desired crystallization temperatures for growth rate and morphological studies. All experiments were carried out under a purge of nitrogen gas.

Small angle light scattering (SALS) experiments were also performed on selected films cast between glass cover slips in order to determine if any differences in nucleation density from sample to sample were apparent. SALS experiments were performed in a light proof room with a He–Ne laser (λ = 6328 Å). An open-back camera was mounted 10 cm from the sample in order to measure the H_v scattering pattern using the method described by Stein[31].

Samples for WAXD experiments were compression moulded into plaques 10 mm in diameter and 0.50 mm thick. All WAXD experiments were performed on a Nicolet diffractometer operating at 40 kV and 30 mA and equipped with a STOE Bragg–Brentano type goniometer. CuK_α radiation of wavelength 1.54 Å was passed through a graphite monochromator prior to final collimation. Data were collected at 0.05° increments for 30 s at each step between the angles of 10° and 35°. Data collection and analysis were performed using the Siemens Polycrystalline Software package.

Thermal analysis

A Seiko DSC 220C equipped with an auto-cooler was used to obtain bulk crystallization information as well as heats of fusion. Prior to all crystallization experiments, samples were heated to 320°C for 4 min. Crystallization from the melt could be observed in the temperature range of 230–270°C. The lower temperature limit was set by the time it took for the d.s.c. signal to stabilize after the auto-cooler rapidly cooled the d.s.c. to the crystallization temperature. The upper limit was set by the long residence times encountered and the resulting limitations with temperature stability and heat transfer. Crystallization experiments from the glass were performed by placing amorphous samples of PPS in the d.s.c. cell which was equilibrated at the crystallization temperature. For the dynamic crystallization experiments, samples were heated to 320°C, held for 4 min, and

subsequently cooled to room temperature at the rate of $10°C\,min^{-1}$. The temperature of the peak of the crystallization exotherm during cooling gives an indication of the crystallization rate. All d.s.c. experiments were carried out under a nitrogen purge.

Rheological experiments

Samples were dried in a vacuum oven for 2 h at 110°C and then compression moulded into 1″ diameter disks approximately 2.5 mm thick. All measurements were performed on an RMS 800 shear rheometer under nitrogen. Samples were heated to 300°C for 8 min prior to data collection to ensure samples had reached thermal equilibrium. Frequency sweeps were performed from 0.1 to $100\,rad\,s^{-1}$ with strain amplitudes on the order of 30%. Four data points were collected for each decade of frequency.

DATA ANALYSIS

Growth rate measurements

Spherulitic growth was followed by taking photomicrographs with a 35 mm camera attached to the polarized optical microscope at fixed time intervals. The spherulite diameters, in μm, were subsequently determined from these photomicrographs. The radius was then plotted as a function of time which provided a straight line with slope equal to the crystalline growth rate, G. The relative error in growth rate measurements was no greater than 5% in most cases.

Small angle light scattering

Undeformed spherulitic structure, evident in many polymers, generally results in a H_v SALS pattern under cross polarized light having fourfold symmetry. This pattern is known as the 'four-leaf clover'[32] pattern. At the intensity maximum of each lobe, the following relationship is satisfied:

$$4.09 = 4\pi R \sin(\Theta_{max}/2)/\lambda_m \qquad (1)$$

In this case R is the weight average spherulite radius, Θ_{max} is the scattering angle at which an intensity maximum is observed, and λ_m is the wavelength of light in the material. In this case λ_m is calculated using 1.7 as the calculated refractive index of PPS from group contribution methods[33], and was also verified experimentally in our laboratory. Since Θ_{max} is easily obtained from photographic measurements, SALS is a rapid means of determining average spherulite size, and since these spherulites fill the volume of the material, SALS may also be used to estimate changes in nucleation densities.

WAXD

WAXD experiments were used to determine the crystalline fraction as a function of molecular weight, using a method similar to that of Hermans and Weidinger[34]. The method of peak deconvolution used in this study has been previously utilized by the authors to determine the crystallinity of LARC CPI[35] and nylon-6[36]. The amorphous scattering profile was obtained from a high molecular weight sample quenched from the melt in ice water. The amorphous scattering profile was then fitted to the total diffracted intensity and then subtracted to yield the scattering due to the crystalline peaks

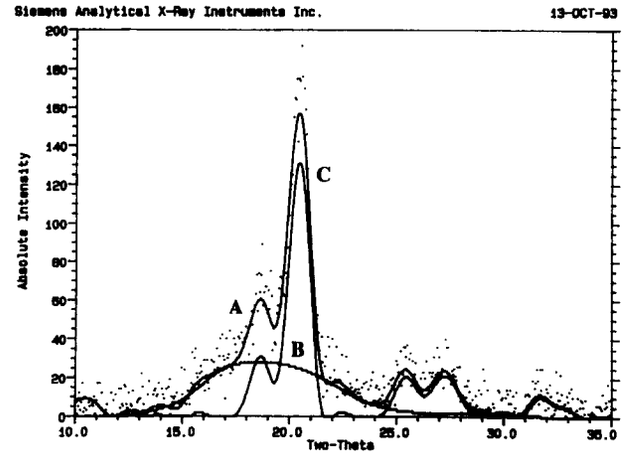

Figure 2 Resolution of WAXD data into amorphous and crystalline components. A, smoothed scattering pattern and raw data (points); B, amorphous scattering profile; C, crystalline peaks

neglecting any effects such as thermal diffuse scattering and scattering from defects. The ratio of the area under the crystalline peaks over the total diffracted intensity gives an estimate of the crystalline fraction. The experimental method of peak deconvolution is outlined in *Figure 2*.

Crystallization kinetics

The overall rate of bulk crystallization may often be analysed in terms of the well-known Avrami equation[37]

$$X_c(t) = 1 - \exp(-Kt^n) \qquad (2)$$

where $X_c(t)$ is the normalized crystalline content at time, t, after the onset of crystallization. K is a rate constant which may be written in terms of the crystal growth rate, G, and the nucleation density, N. The Avrami exponent, n, is a term dependent on the types of processes occurring during nucleation and growth. Assuming three-dimensional growth, it can be shown that[38]

$$K = 4\pi NG^3/3 \qquad (3)$$

By rearranging and taking the double logarithm of equation (2) we obtain

$$\ln[-\ln(1 - X_c(t))] = \ln K + n \ln t \qquad (4)$$

Thus a plot of the double logarithm of amorphous content as a function of ln(time), a classical Avrami plot, gives a straight line with slope n and intercept $\ln K$. An alternative method of obtaining the same information involves the use of crystallization half-times. In this case the entire area under the crystallization exotherm represents a normalized crystalline content of unity. On a normalized basis the crystallization half-time, $t_{1/2}$ is defined as the time at which the normalized crystalline content is 0.5. From a graph of normalized crystalline content vs ln (time) one may determine the Avrami exponent, n from the slope at $t = t_{1/2}$.

Taking the logarithm of equation (2) at $t = t_{1/2}$ one obtains[39]

$$K = \ln(2)/t_{1/2}^n \qquad (5)$$

The slope, S, of the curve $(1 - X_c(t))$ as a function of ln(time) may be written as:

$$S = t[\delta(1 - X_c(t))]/\delta t \qquad (6)$$

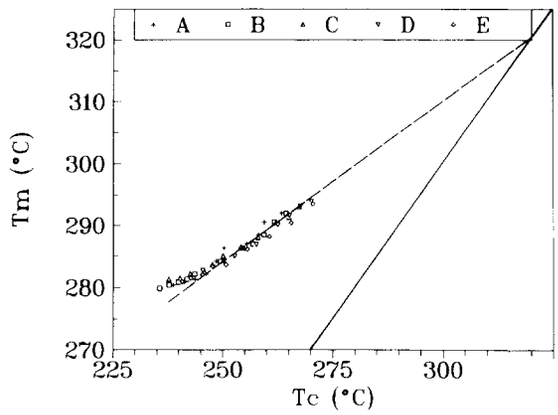

Figure 3 Hoffman–Weeks plots used to determine the thermodynamic melting temperatures of various PPS samples as a function of molecular weight and endgroup counter-ion. A, Parent #2: $\langle M_w \rangle = 44000$; B, Parent #1: $\langle M_w \rangle = 64000$; C, Na^+ washed Fraction #2: $\langle M_w \rangle = 57000$; D, Zn^{2+} washed Fraction #2: $\langle M_w \rangle = 60000$; E, Acid washed Fraction #2: $\langle M_w \rangle = 54000$

From equation (2) $\delta(1 - X_c(t))/\delta t$ may be calculated:

$$\delta(1 - X_c(t))/\delta t = -Knt^{n-1} \exp(-Kt^n) \quad (7)$$

at $t = t_{1/2}$

$$S_{t1/2} = n \ln(2)/2 \quad (8)$$

RESULTS AND DISCUSSION

When determining the crystallization behaviour of a polymer, it is important, when possible, to estimate the equilibrium melting point in order to know whether the melt hold temperature is above or below the equilibrium melting point. If the melt hold temperature is not well above the equilibrium melting point, residual nuclei may survive in the melt. The method of Hoffman and Weeks[40] was used to obtain the equilibrium melting points, T_m°, of all specimens investigated in this study.

In an earlier study[13], López and Wilkes found that the extrapolated values for equilibrium melting points of PPS varied somewhat as a function of molecular weight. In this earlier study, instrumental sensitivity limited the maximum temperature for crystallization to approximately 265°C, and the extrapolation was performed from crystallization temperatures in the range 250–265°C.

Since the earlier work of López and Wilkes, Cebe and Chung have demonstrated that substantial reorganization may occur in PPS crystals especially as crystals grown under conditions of high undercoolings are melted[41,42]. In such a case significant deviations from linearity in Hoffman–Weeks plots may be observed especially when crystals formed at conditions of high undercoolings are melted. Due to greater instrumental sensitivity for the experiments performed in this study, data were extrapolated in the temperature range 255–270°C. The Hoffman–Weeks plot obtained for PPS samples of varying molecular weight, polydispersity, and endgroup counter-ion is shown in *Figure 3*. Apparent deviations from linearity are obtained at temperatures as high as 255°C. In this study, extrapolations performed on data obtained in the 255–270°C range produced equilibrium melting points of 320 ± 2°C for all samples regardless of molecular weight or the chemical nature of the endgroup counter-ion.

Table 3 Result of SALS patterns obtained from PPS with varying $\langle M_w \rangle$

$\langle M_w \rangle$	Θ_{max} (°)	Average spherulite radius (μm)
44000	4.6	3.0
56000	8.5	1.6
64000	13.0	1.1
104000	16.7	0.8

López *et al.* showed an increase in the equilibrium melting temperature of 8°C over an increase of *ca.* 39 K ($\langle M_w \rangle = 24000$ to $\langle M_w \rangle = 63000$) in weight average molecular weight[13]. Lovinger *et al.*[12] reported an increase of 12°C in the equilibrium melting temperature on going from $\langle M_w \rangle = 15000$ to $\langle M_w \rangle = 51000$. Cebe *et al.* reported a 30°C increase in the equilibrium melting temperature when $\langle M_w \rangle$ increased from 15000 to 60000[41,42]. A common feature of these earlier studies is that T_m° varied when the variation of molecular weight was in the range of *ca.* 15000 to *ca.* 60000. In this study, however, the variation of molecular weight was from $\langle M_w \rangle = 44000$ to $\langle M_w \rangle = 64000$. Though an increase in equilibrium melting temperature with molecular weight is to be expected on theoretical grounds, it is likely that in this narrow molecular weight range the equilibrium melting temperature is only weakly dependent on molecular weight.

SALS

The nucleation density was observed to vary somewhat as a function of molecular weight for the PPS samples used in this study. SALS patterns for PPS samples crystallized at 245°C with $\langle M_w \rangle = 44000$, $\langle M_w \rangle = 56000$, $\langle M_w \rangle = 64000$, and $\langle M_w \rangle = 104000$ are shown in *Figure 4*. For PPS crystallized at 245°C, the spherulites in the lowest molecular weight PPS specimen grew to be about four times as large as those for the highest molecular weight PPS specimen. From the change in SALS patterns it is apparent that a distinct difference in weight average spherulite radius exists for different molecular weight PPS samples crystallized with identical thermal histories. By combining the data from *Figure 4* with equation (1) the weight average spherulite radius may be calculated as a function of molecular weight. These results are summarized in *Table 3*. Since more than adequate time was given for impingement of spherulites and completion of crystallization in each case, the much smaller average spherulite radius corresponds to a much higher nucleation density in the higher molecular weight species. In fact according to first order calculations based on the results of the SALS patterns, *the nucleation density of the high molecular weight PPS is nearly 50 times that of the low molecular weight PPS crystallized under identical conditions.*

Crystal growth rate

Linear crystal growth rate data were obtained from observing the radius of growing spherulites from optical micrographs at set time intervals (*Figure 5*). These data were then plotted as spherulite radius as a function of time. Since different spherulites may nucleate at different times and the start of the timing for the experiment is

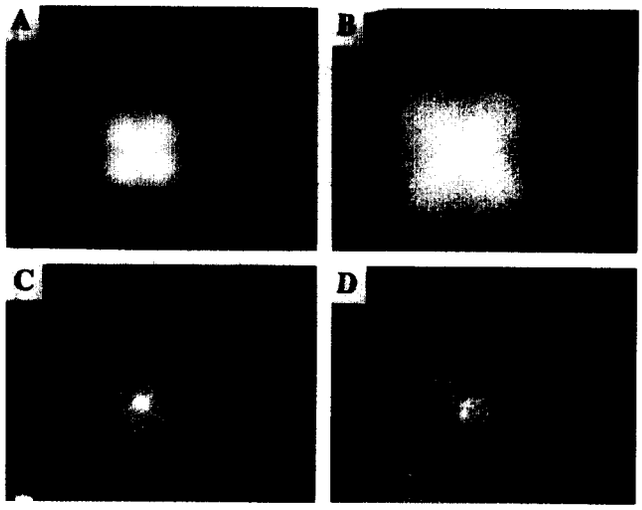

Figure 4 SALS patterns obtained from PPS. A, $\langle M_w \rangle = 44\,000$; B, $\langle M_w \rangle = 56\,000$; C, $\langle M_w \rangle = 64\,000$; D, $\langle M_w \rangle = 104\,000$

arbitrary, not all plots intercept the origin. One such plot is shown in *Figure 6*, the slope of which provides the linear crystalline growth rate. Crystal growth rate as a function of endgroup counter-ion and temperature for fractionated PPS with $\langle M_w \rangle = 56\,000$ is plotted in *Figure 7. All species which had undergone the Na^+ or Zn^{2+} ion-exchange process or had been acid washed, had a crystalline growth rate at least one log unit more rapid than the untreated fractionated sample*. For the species which had undergone the ion-exchange or acid wash process, the growth rates decreased in the following order: $H^+ > Zn^{2+} > Na^+$. López *et al.*[14] observed that the growth rate of the Na^+ exchanged sample was the same as that of the unfractionated as-received sample, and the growth rates decreased in the same order as a function of endgroup counter-ion as observed in this study. However, since this study was carried out on fractionated samples, thus having a lower fraction of endgroups, it can be deduced that effective exchange of Na^+ ions does indeed alter the growth rate behaviour, when the effect of other endgroup ions is minimized. It is known that the growth rate depends on the transport and secondary nucleation processes. It was hypothesized in the previous study by López *et al.*[14] that the transport term was likely unaffected by the endgroup counter-ion and that changes in secondary nucleation was caused by different endgroup counter-ions, which resulted in different growth rates. The rheological data obtained in the previous study seemed to be consistent with this interpretation. The rheological experiments carried out by us, and discussed in the next section shed some light on this aspect as well.

Growth rates for the higher molecular weight fraction as well as the ion-exchanged high molecular weight fractions were not attainable due to the much higher nucleation densities and thus much smaller average spherulite sizes observed in these systems, thereby limiting optical measurements. The higher nucleation densities in these systems is likely due to the fairly low melt temperature used and the inability to fully destroy residual order in the melt due to longer relaxation times. However, melt hold temperatures as high as 365°C and hold times as long as 10 min, still did not allow growth rate measurements, and caused the SALS patterns to become more diffuse, but remain about the same size,

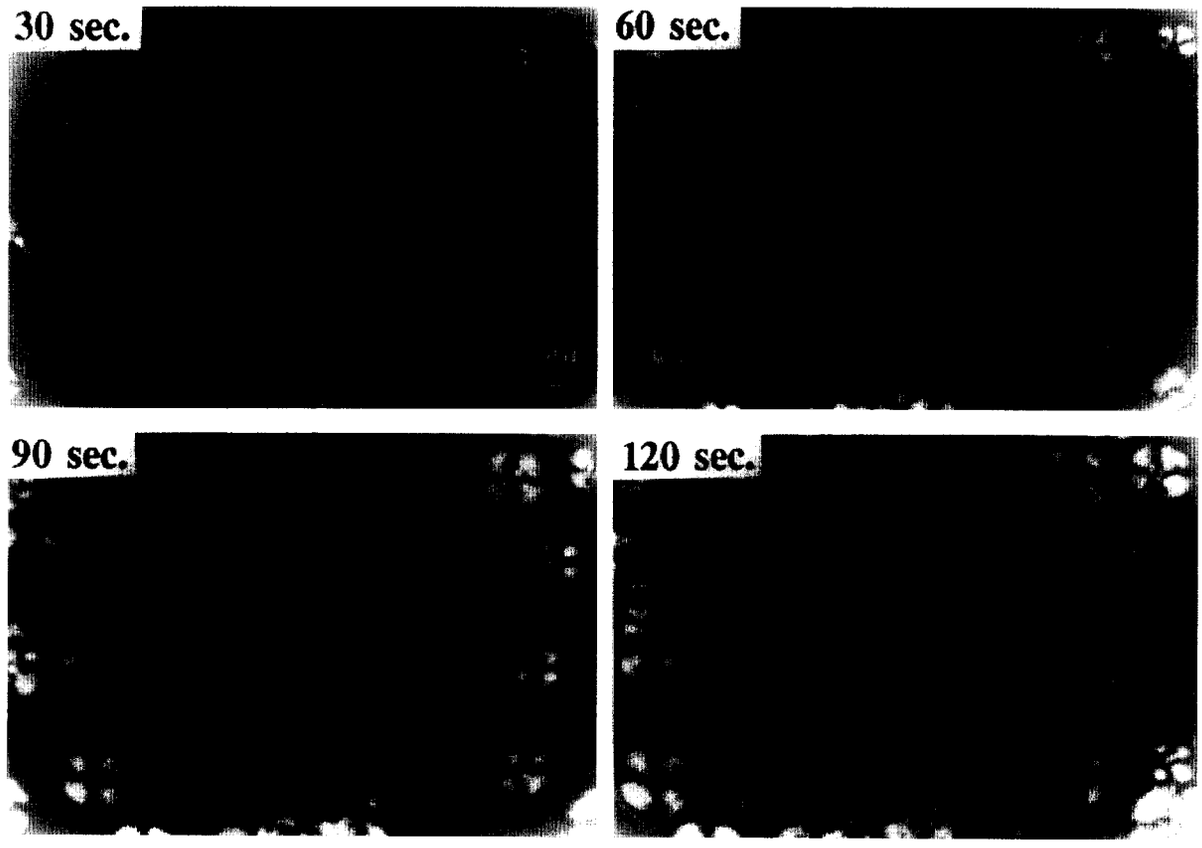

Figure 5 Optical micrographs of PPS with $\langle M_w \rangle = 56\,000$ as a function of increasing crystallization time

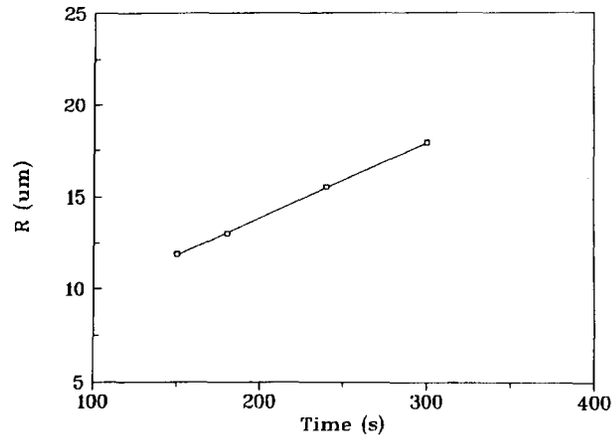

Figure 6 Data used to determine growth rate data for PPS

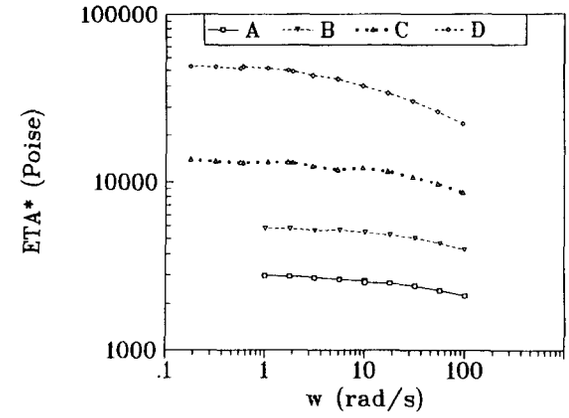

Figure 8 Shear viscosity of PPS as a function of frequency at 300°C for PPS. A, $\langle M_w \rangle = 44000$; B, $\langle M_w \rangle = 56000$; C, $\langle M_w \rangle = 64000$; D, $\langle M_w \rangle = 104000$

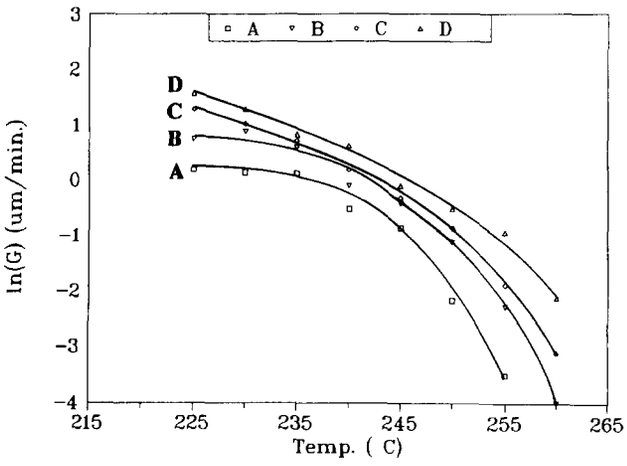

Figure 7 Crystal growth rates as a function of endgroup counter-ion and temperature for fractionated PPS with $\langle M_w \rangle = 56000$. A, fractionated; B, Na^+ washed; C, Zn^{2+} washed; D, acid washed

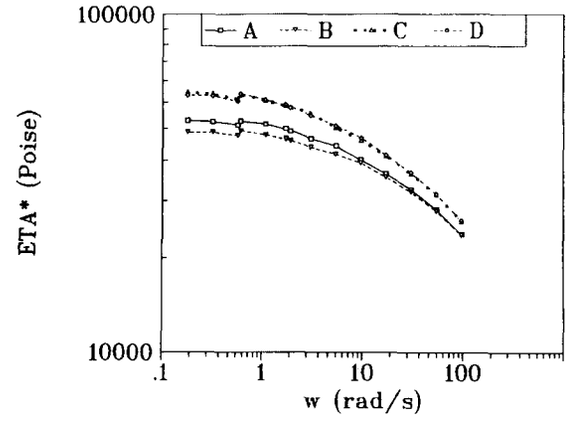

Figure 9 Shear viscosity of PPS with $\langle M_w \rangle = 104000$ as a function of frequency at 300°C. A, fractionated; B, acid washed; C, Zn^{2+} washed; D, Na^+ washed

thereby implying that the nucleation density was relatively unchanged.

Rheological behaviour

The viscoelastic behaviour of commercially available Ryton® PPS has been studied earlier by Eisenberg and Cayrol[43] to temperatures as high as 340°C, but a systematic study investigating the effects of ionic interactions in PPS has not previously been undertaken. Frequency sweeps were performed on all of the PPS specimens under a nitrogen atmosphere at 300°C at frequencies from 0.1 to 100 rad s^{-1}. As expected the viscosity of these specimens increased with molecular weight (*Figure 8*).

For both the high molecular weight and low molecular weight fractions there were distinct trends in viscosity as a function of endgroup counter-ion (*Figures 9* and *10*). It is worth noting that the acid washed specimens for both molecular weights displayed the lowest viscosities—particularly at the lower frequencies. Recall also that the acid washed specimens exhibited the highest growth rates at all the temperatures investigated in this study as shown in *Figure 7*. The Na^+ and Zn^{2+} washed samples exhibited slightly higher viscosities as compared to the fractionated sample and the acid washed sample, particularly at lower frequencies. Note, however, that the scales on these latter two plots are expanded, so the differences while real are not extreme. It is recalled that the growth rate studies, however, showed that the Na^+ and Zn^{2+} washed samples exhibited higher growth rates as compared to the fractionated sample. The variation in growth rate can thus be at least partially attributed to the differences in the transport process during crystallization.

The trends in viscosity may be explained by secondary interactions due to association through ionic endgroups. The unexchanged polymer has whatever ions are present after polymerization. The acid wash process was developed to specifically remove the metal ions and protonate ionizable endgroups; therefore the acid washed species exhibited less ionic interaction through decreased viscosity. The Na^+ and Zn^{2+} washed polymers had ionic species reintroduced and therefore exhibited a greater degree of association through increased viscosity. Melt rheological data associated with these materials is summarized in *Table 2*.

Crystallization kinetics

Data from the isothermal crystallization experiments were put in the format for crystallization half-time analysis (*Figures 11A–D*) as well as classical Avrami analysis (*Figures 12A–D*). *Figure 11* shows plots of normalized crystalline content as a function of ln(time)

for PPS with $\langle M_w \rangle = 44\,000$ and $\langle M_w \rangle = 104\,000$ for both melt and cold crystallized data. From these data and equations (5) and (8), the Avrami exponents, n, and rate constants, K, were determined as a function of temperature. Analysis of the Avrami plots (*Figure 12*) using equation (4) yielded the n and K values from the slope and the inverse log of the intercept.

Both crystallization half-times analysis and Avrami analysis were performed on data for all specimens over the temperature ranges of 110–125°C and 230–270°C. The results obtained by these two separate techniques were essentially identical. Avrami exponents were found to vary between 2 and 3 depending on molecular weight and crystallization temperature. The higher molecular weight parent had an Avrami exponent value of nearly 3 at all crystallization temperatures whereas the low molecular weight parent had an Avrami exponent close to 2 (*Figure 13*). In both cases, fractionation reduced the Avrami exponent. There is also a trend for slightly reduced Avrami exponents at lower crystallization temperatures, possibly due to the inability for well developed spherulites to form before impingement occurs.

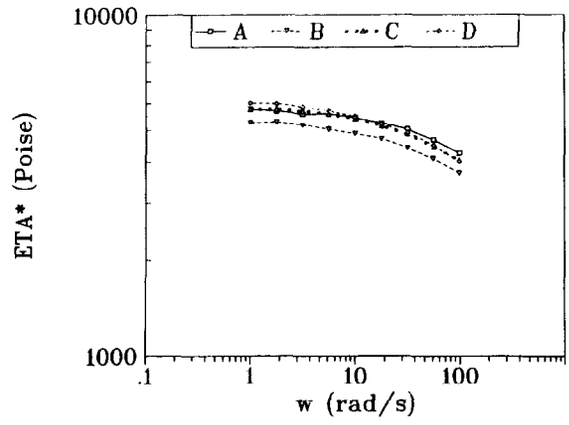

Figure 10 Shear viscosity of PPS with $\langle M_w \rangle = 56\,000$ as a function of frequency at 300°C. A, fractionated; B, acid washed; C, Zn^{2+} washed; D, Na^{+} washed

The effects of fractionation and the chemical nature of the endgroup counter-ion on crystallization rate constants and half-times for Parent #1 and Fraction #1 as well as the respective ion-exchanged samples are illustrated in *Figure 14*. For the high molecular weight species, the unfractionated sample (Parent #1) with $\langle M_w \rangle = 64\,000$ crystallized more rapidly than the fractionated sample (Fraction #1) with $\langle M_w \rangle = 104\,000$ in the nucleation controlled temperature regime, but in the diffusion controlled temperature range the opposite trend was observed. This trend may be due to the fact that ionic association of endgroups may be stronger at lower temperatures, which could promote a higher melt viscosity, and lead to a depression in nucleation density. Since a parent sample would have a higher concentration

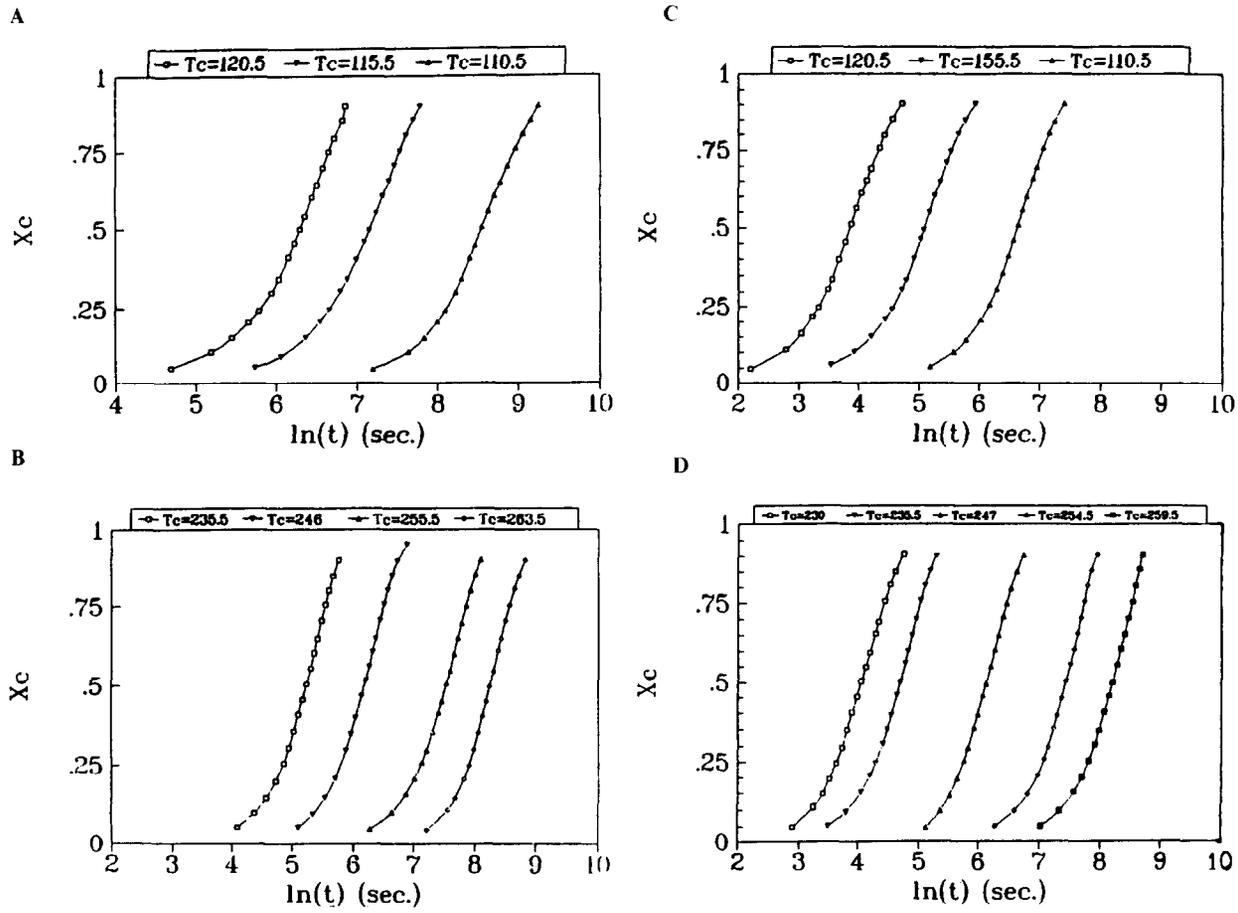

Figure 11 Normalized crystalline content, X_c vs ln(time) for PPS with: (A) $\langle M_w \rangle = 44\,000$; diffusion controlled temperature range. (B) $\langle M_w \rangle = 44\,000$; nucleation controlled temperature range. (C) $\langle M_w \rangle = 104\,000$; diffusion controlled temperature range. (D) $\langle M_w \rangle = 104\,000$; nucleation controlled temperature range

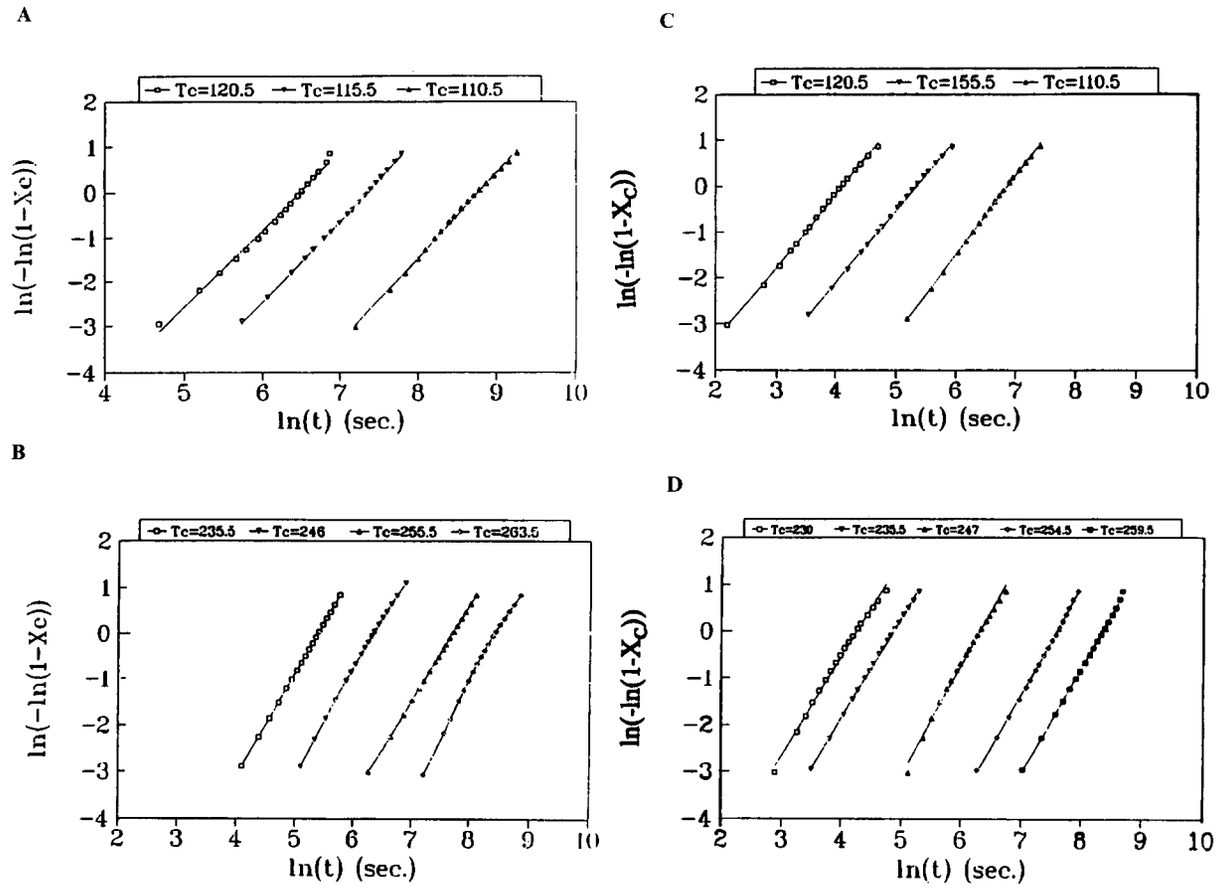

Figure 12 Avrami plots for PPS with: (A) $\langle M_w \rangle = 44\,000$; diffusion controlled temperature range. (B) $\langle M_w \rangle = 44\,000$; nucleation controlled temperature range. (C) $\langle M_w \rangle = 104\,000$; diffusion controlled temperature range. (D) $\langle M_w \rangle = 104\,000$; nucleation controlled temperature range

of endgroups, this effect would be stronger for the parent as compared to the fractionated sample. Since fractionation would greatly reduce the concentration of ionic endgroup species, the fractionated sample would crystallize more rapidly from the glass than the parent sample. The acid washed sample with $\langle M_w \rangle = 104\,000$ crystallized more rapidly than the Na^+ and Zn^{2+} exchanged samples in both temperature ranges.

The effects of both fractionation and the chemical nature of the endgroup counter-ion were distinctly more substantial for the low molecular weight species. As illustrated in *Figure 15*, the fractionated species with $\langle M_w \rangle = 56\,000$ crystallized more rapidly than the parent species with $\langle M_w \rangle = 44\,000$, which again could be due to endgroup association reducing the crystallization rate. The effects of endgroup counter-ion for the low molecular weight system were again more substantial than for the higher molecular weight species. *All the species which had undergone the ion-exchange process crystallized more rapidly than the fractionated sample which had not undergone the process.* The rates of bulk crystallization decreased in the following order: $H^+ > Zn^{2+} > Na^+$. This result is consistent with the finding that the acid washed specimens exhibited higher growth rates as compared to the Na^+ or Zn^{2+} washed samples. These trends are also consistent with those observed by López *et al.* in their earlier study[14].

Nucleation density

The nucleation density can be calculated from the Avrami rate parameter K, the Avrami exponent n, and

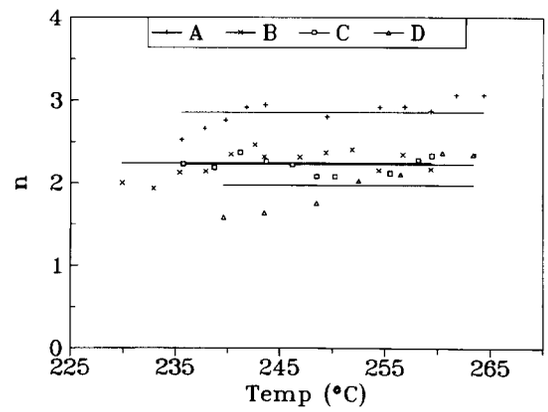

Figure 13 Avrami exponents as a function of molecular weight. A, Parent #1: $\langle M_w \rangle = 64\,000$; B, Fraction #1: $\langle M_w \rangle = 104\,000$; C, Parent #2 $\langle M_w \rangle = 44\,000$; D, Fraction #2 $\langle M_w \rangle = 56\,000$

the growth rate G data. Since a wide range of Avrami exponent values (2–3) were obtained, a rigorous calculation of the nucleation density does not seem justified. However, a calculation of the nucleation density with a constant exponent value of 3 was carried out for the purposes of comparison. The calculation showed that the nucleation density was weakly affected by the nature of the counter-ion, and was similar to the value for the fractionated polymer. This contrasts with the earlier finding by López *et al.*[14] on unfractionated samples which showed that the nucleation density

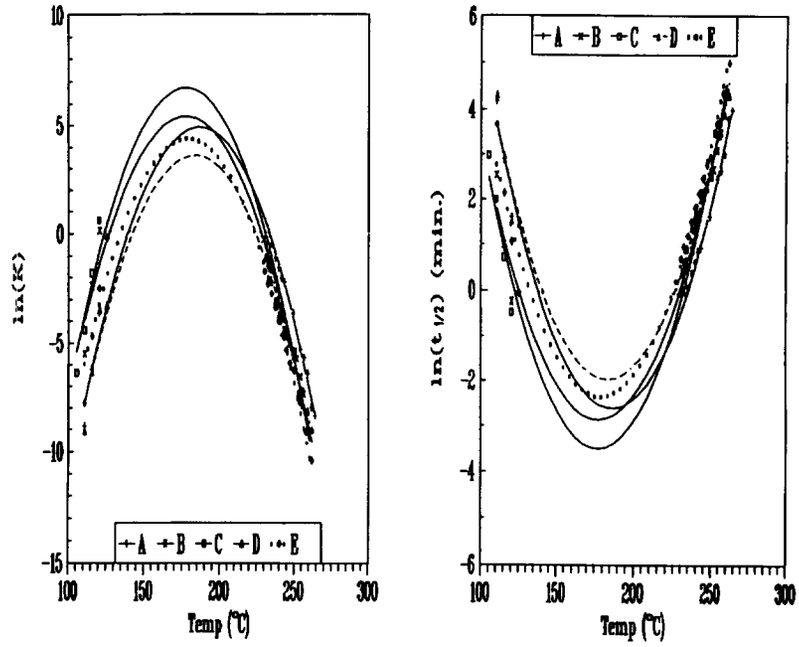

Figure 14 Effects of fractionation and endgroup counter-ion on crystallization half-times, $t_{1/2}$, and ln(K) for HMW PPS. A, Parent #1: $\langle M_w \rangle$ = 64 000; B, Fraction #1: $\langle M_w \rangle$ = 104 000; C, Acid washed Fraction #1; D, Na^+ washed Fraction #1; E, Zn^{2+} washed Fraction #1

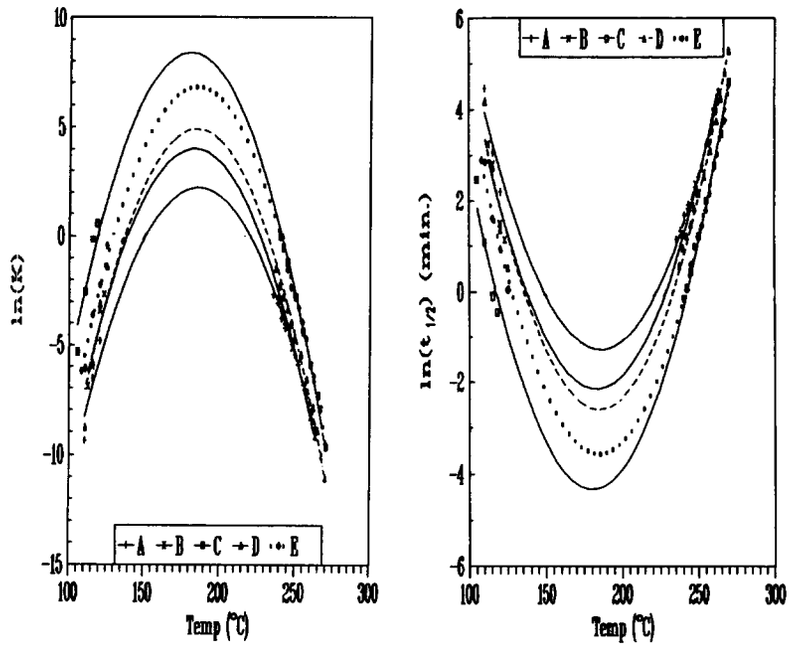

Figure 15 Effects of fractionation and endgroup counter-ion on crystallization half-times, $t_{1/2}$, and ln(K) for LMW PPS. A, Parent #2: $\langle M_w \rangle$ = 44 000; B, Fraction #2: $\langle M_w \rangle$ = 56 000; C, Acid washed Fraction #2; D, Na^+ washed Fraction #2; E, Zn^{2+} washed Fraction #2

increased by at least 20 times on introduction of different counter-ions. Since this was not observed in this study, this lack of dependency of the nucleation density on the counter-ion can be explained as being due to the lower fraction of endgroups utilized in this study. Clearly, however, the result of both these studies establishes that both the concentration as well as the nature of the endgroup counter-ion affects the nucleation density and therefore the bulk crystallization kinetics of PPS.

As was mentioned in the Experimental section, some samples of the lower molecular weight fraction were subjected to repeated acid wash and Na^+ exchange reactions in order to confirm that the ion-exchange reactions involving the endgroups were indeed reversible. In order to confirm this hypothesis, three samples (Na1, Acid wash2 and Na2) were analysed by d.s.c. and optical microscopy in order to investigate the crystallization behaviour and morphology of these samples.

Dynamic crystallization experiments were carried out on the samples, that each had been melted by the

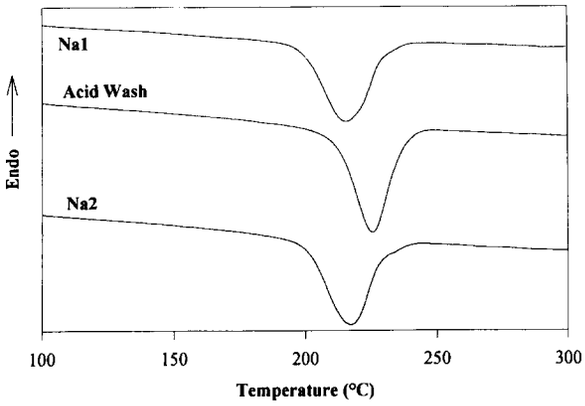

Figure 16 D.s.c. thermograms showing cooling curves of fractionated PPS ($\langle M_w \rangle = 56\,000$) samples with Na^+ and acid counter-ions

procedures described earlier, and by cooling the samples at $10°C\,min^{-1}$. The d.s.c. scans showing the crystallization exotherms on cooling are shown in *Figure 16*. The temperature at the peak of the crystallization exotherm (T_{cmax}) is a function of the rate of crystallization of the system. A larger value of T_{cmax} clearly verifies that crystallization occurs at smaller undercoolings, which therefore indicates faster crystallization at any given undercooling. This faster rate of bulk crystallization could occur due to increased growth rate and/or increased nucleation density. As can be seen in *Figure 16*, the acid wash system crystallized at lower undercoolings, while the two Na^+ samples (Na1 and Na2) crystallized at essentially the same temperature, *indicating that the ion-exchange process was indeed reversible*. The faster crystallization rate of the acid wash system as compared to the Na^+ exchanged system is consistent with the earlier result which showed a higher spherulitic growth rate for the acid wash system as compared to the Na^+ sample (*Figure 7*).

In order to study the effects of endgroup counter-ion on the nucleation density of these same materials, these three samples were then crystallized at 260°C for 5 h, the optical micrographs of which are shown in *Figure 17*. From the figure it is apparent that the Na^+ exchanged samples (Na1 and Na2) exhibit similar if not identical nucleation densities, which again reinforces the hypothesis that the counter-ions can be reversibly exchanged. The micrographs of the Na^+ samples show distinct, isolated spherulites which even after 5 h at 260°C had not completely filled the volume, indicating distinctly slower kinetics. In contrast, the micrograph of the acid washed sample does not exhibit any distinct spherulites, rather the whole volume exhibits a grainy birefringent pattern which is indicative of very high nucleation density and consequently very small spherulite sizes. It is thus apparent that the acid washed specimens exhibit a considerably higher nucleation density than the Na^+ exchanged samples. The faster bulk crystallization kinetics observed for the acid washed system is thus a result of increased nucleation density *and* higher growth rates. This finding is also consistent with the earlier finding of López *et al.*, who calculated the nucleation densities from the Avrami parameters and growth rate data and observed that the acid washed system exhibited considerably higher nucleation density than the Na^+ washed system, in low molecular weight unfractionated PPS.

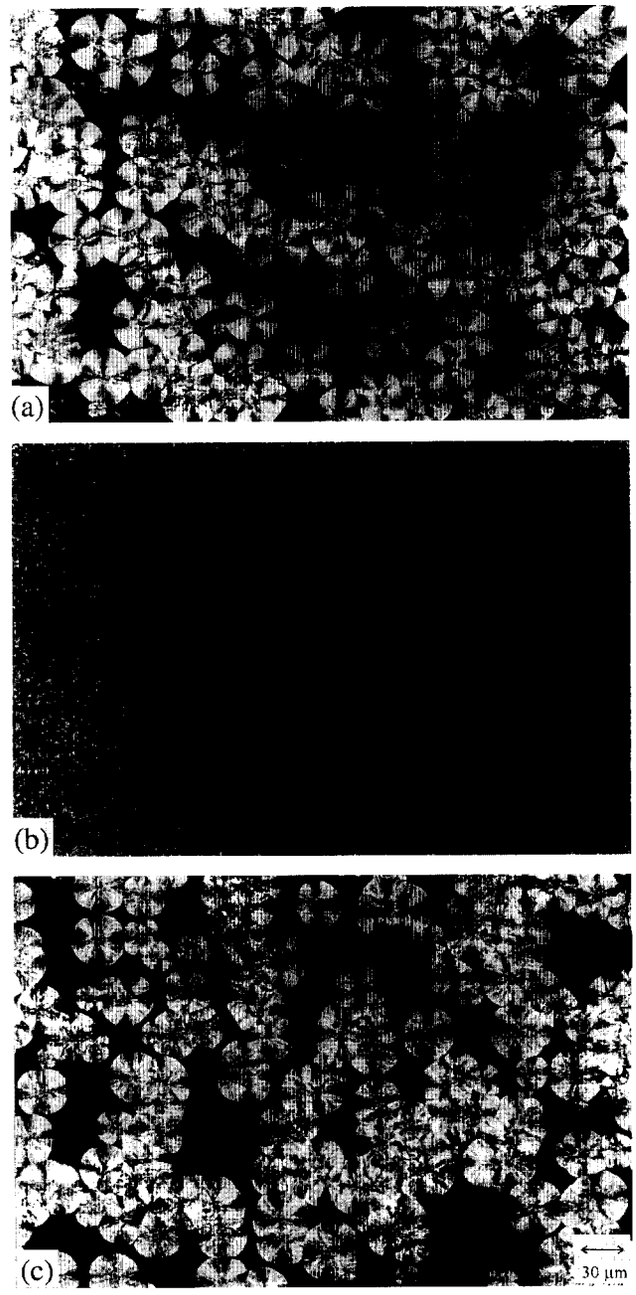

Figure 17 Optical micrographs of fractionated PPS samples ($\langle M_w \rangle = 56\,000$) with Na^+ and acid counter-ions. A, Na1; B, Acid washed; C, Na2

Determination of crystallinity

The heat of bulk crystallization was measured for all samples which were crystallized from the melt. *Figure 18* illustrates the strong dependence of the heat of crystallization on molecular weight. The higher molecular weight species showed consistently lower heats of crystallization indicating a lower level of crystallinity in these samples. This effect was most noticeable for the fraction with $\langle M_w \rangle = 104\,000$. The effects of the chemical nature of the counter-ions on the heats of crystallization were also measured. For the high molecular weight fraction no significant effects of endgroup counter-ion were observed on the heat of crystallization (*Figure 19A*). It is likely that no endgroup counter-ion effect is observed in the high molecular weight species due to the fact that the concentration of the endgroups in this

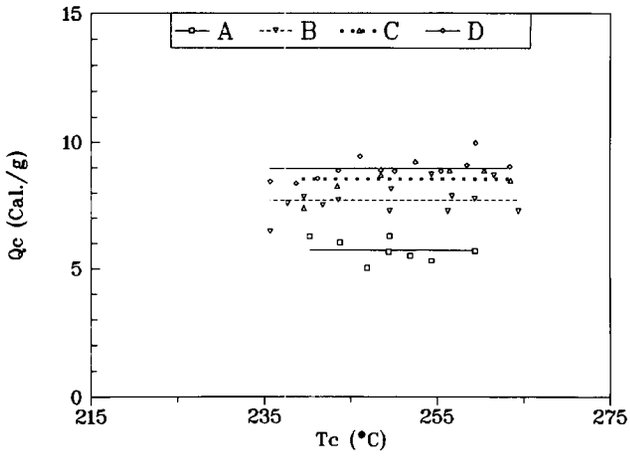

Figure 18 Effect of molecular weight on the bulk heat of crystallization for PPS crystallized from the melt. A, $\langle M_w \rangle = 104\,000$; B, $\langle M_w \rangle = 64\,000$; C, $\langle M_w \rangle = 56\,000$; D, $\langle M_w \rangle = 44\,000$

fraction is very low, which is consistent with data presented earlier. For the low molecular weight fraction, the acid washed specimens showed a reduced heat of crystallization at higher undercoolings (*Figure 19B*). *Table 4* summarizes the data obtained from the heat of crystallization measurements.

The effects of molecular weight on the degree of crystallinity was also investigated by WAXD. *Figure 20* illustrates the WAXD patterns obtained from species with varying molecular weight crystallized at 250°C for 2 h. At this temperature, 2 h was more than adequate time for these samples to reach their maximum value of crystallinity. A systematic decrease in the crystalline fraction was observed with increasing molecular weight—see *Table 5*. A similar trend was noted in heats of melting for samples crystallized under identical conditions.

CONCLUSIONS

The effects of fractionation and the chemical nature of the endgroup counter-ion for PPS samples of varying molecular weight on the crystallization behaviour of PPS were investigated. The equilibrium melting temperature was determined for all samples to be 320 ± 2°C, and independent of molecular weight and nature of endgroup counter-ion. The nucleation density of PPS increased with increasing molecular weight, likely due to the fact that residual order survived the melt treatment in this system. Growth rates determined for PPS with $\langle M_w \rangle = 56\,000$ as a function of endgroup counter-ion were found to decrease in the following order: $H^+ > Zn^{2+} > Na^+ >$ untreated fractionated sample. The ion-exchange process used in this study also increased the rate of bulk crystallization relative to samples which had not undergone the ion-exchange process. In all cases the acid washed samples were found to crystallize most rapidly. For the low molecular weight samples, this was shown to be due to an increase in both the growth rate as well as nucleation density. The effects of fractionation and the ion-exchange process were much more pronounced in the lower molecular weight species than in the high molecular weight PPS, probably due to the lower

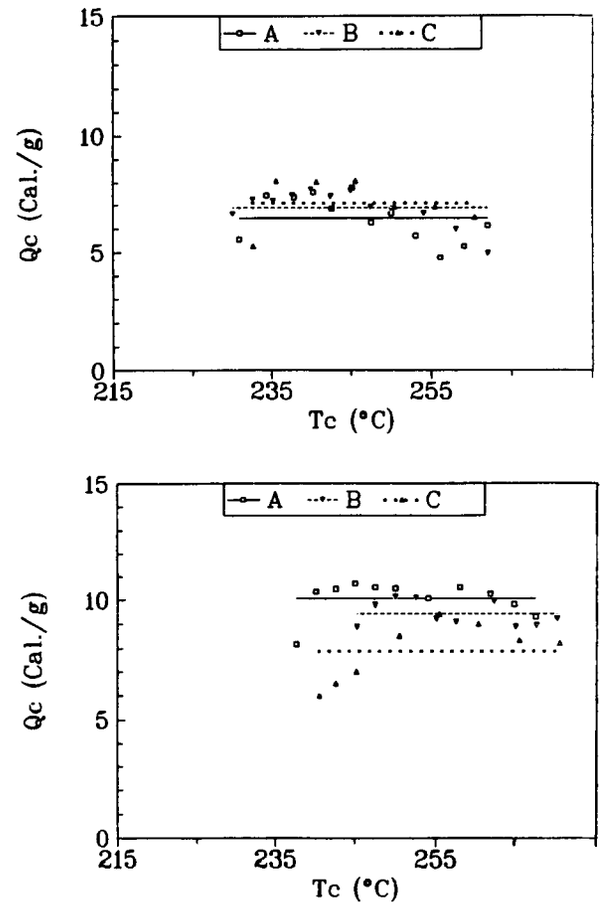

Figure 19 Effect of endgroup counter-ion on the bulk heat of crystallization for: (A) PPS with $\langle M_w \rangle = 104\,000$. A, Na^+ washed; B, Zn^{2+} washed; C, acid washed. (B) PPS with $\langle M_w \rangle = 56\,000$. A, Na^+ washed; B, Zn^{2+} washed; C, acid washed

Table 4 Average values of heats of crystallization for PPS as a function of molecular weight and endgroup counter-ion

$\langle M_w \rangle$	Endgroup counter-ion	Average ΔQ_c (J g^{-1})
104 000	Unexchanged	6.9
	Na^+	6.5
	Zn^{2+}	6.9
	Acid	7.0
64 000	Unexchanged	8.8
56 000	Unexchanged	10.1
	Na^+	10.1
	Zn^{2+}	9.5
	Acid	7.9
44 000	Unexchanged	10.5

fraction of endgroups in the higher molecular weight systems.

Since a strong effect on the crystallization behaviour was noted in an earlier study by some of the co-authors on unfractionated PPS of similar molecular weight, it was proposed that aggregates of ionic endgroups could enhance nucleation. Since the number of ionic endgroups is greatly decreased due to the fractionation process used in this study, the effect of endgroup counter-ion on nucleation is probably greatly reduced, although the acid washed low molecular weight fractionated sample was shown to have a higher nucleation density than the Na^+ exchanged sample. The reversibility of the ion-exchange reactions was established by the results of d.s.c. and

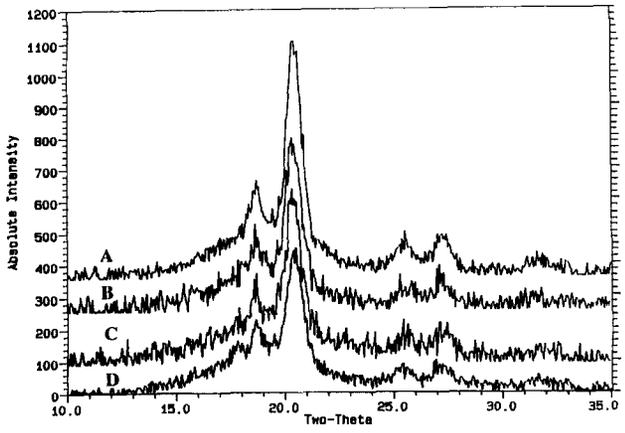

Figure 20 WAXD patterns of PPS crystallized at 250°C for 2 h. A, $\langle M_w \rangle = 44\,000$; B, $\langle M_w \rangle = 56\,000$; C, $\langle M_w \rangle = 64\,000$; D, $\langle M_w \rangle = 104\,000$

Table 5 Results of WAXD absolute crystallinities and d.s.c. heats of melting for samples crystallized at 250°C

$\langle M_w \rangle$	Crystallinity (WAXD) (%)	Heat of melting (d.s.c.) (cal g^{-1})
104 000	35	8.31
64 000	48	10.61
56 000	50	11.05
44 000	53	11.75
Amorphous sample $\langle M_w \rangle = 104\,000$	0	0

optical microscopy studies. Samples with Na^+ counter-ions were exchanged with H^+ counter-ions and exchanged again with Na^+ counter-ions. The behaviour of these two Na^+ exchanged samples were essentially identical by d.s.c. and optical microscopy, implying reversibility of the ion-exchange process. A significant decrease in crystallinity with increasing molecular weight was observed through WAXD experiments, as well as through measurements of melting by d.s.c.

ACKNOWLEDGEMENTS

The authors would like to acknowledge the assistance of Jerold D. Wood for the high temperature g.p.c. measurements. One of the authors (SS) would like to thank the NSF Science and Technology Center for High Performance Polymeric Adhesives and Composites for partial funding under contract # DMR 9120004. This same author would also like to thank Phillips Petroleum Company for fellowship support.

REFERENCES

1 Short, J. N. and Hill, H. W., Jr. *Chem. Technol.* 1972, **2**, 481
2 Hill, W. H., Jr. and Brady, D. G. *Polym. Eng. Sci.* 1976, **16**, 832
3 Ma, C. M., O'Connor, J. E. and Lou, A. Y. *SAMPE Q.* 1984, **15**, 12
4 Hill, H. W., Jr. *Ind. Eng. Chem. Prod. Res. Dev.* 1979, **18**, 4
5 Brady, D. G. *J. Appl. Polym. Sci., Appl. Polym. Symp.* 1981, **36**, 231
6 Shue, R. S. *Dev. Plast. Technol.* 1985, **2**, 259
7 Clarke, T. C., Kanazawa, K. K., Lee, V. Y., Rabolt, J. F., Reynolds, J. R. and Street, G. B. *J. Polym. Sci., Polym. Phys. Edn.* 1982, **20**, 117
8 Frommer, J. E., Elsenbaumer, R. L., Eckhardt, H. and Chance, R. R. *J. Polym. Sci., Polym. Lett. Edn.* 1983, **21**, 39
9 Schoch, K. F., Jr., Chance, J. F. and Pfeiffer, K. E. *Macromolecules* 1985, **18**, 2389
10 Jog, J. P. and Nadkarni, V. M. *J. Appl. Polym. Sci.* 1985, **30**, 997
11 Jog, J. P. and Ravindranath, K. *J. Appl. Polym. Sci.* 1993, **49**, 1395
12 Lovinger, A. J., Davis, D. D. and Padden, F. J., Jr. *Polymer* 1985, **26**, 1595
13 López, L. C. and Wilkes, G. L. *Polymer* 1988, **29**, 106
14 López, L. C., Geibel, J. F. and Wilkes, G. L. *Polymer* 1989, **30**, 147
15 López, L. C. Ph.D. Dissertation, VPI & SU, Blacksburg, VA, 1987
16 López, L. C. and Wilkes, G. L. *Polymer* 1989, **30**, 882
17 Fahey, D. and Ash, C. E. *Macromolecules* 1991, **24**, 4242
18 Wade, B., Abhiraman, A. S., Wharry, S. and Sutherlin, D. *J. Polym. Sci., Part B: Polym. Phys.* 1990, **28**, 1233
19 Reents, W. D., Jr. and Kaplan, M. L. *Polymer* 1982, **23**, 310
20 Novi, M., Petrillo, G. and Sartirana, M. L. *Tetrahedron Lett.* 1986, **27**, 6129
21 Percec, V., Clough, R. S., Rinaldi, P. L. and Litman, V. E. *Macromolecules* 1994, **27**, 1535
22 Menczel, J. D. and Collins, G. L. *Polym. Eng. Sci.* 1992, **32**, 1264
23 Collins, G. L. and Menczel, J. D. *Polym. Eng. Sci.* 1992, **32**, 1270
24 Brady, D. G. *J. Appl. Polym. Sci.* 1976, **20**, 2541
25 Mehl, N. A. and Rebenfeld, L. *Polym. Eng. Sci.* 1992, **32**, 1451
26 Campbell, R. W. U.S. Patent 3,919,177 to Phillips Petroleum Company (November 11, 1975)
27 Stacy, C. J. *J. Appl. Polym. Sci.* 1986, **32**, 3959
28 Scoggins, L. E. and Munro, B. L. U.S. Patent 4,415,729 to Phillips Petroleum Company (November 15, 1983)
29 Saunders, W. E. and Stalder, W. L. U.S. Patent 3,478,000 to Phillips Petroleum Company (November 11, 1969)
30 Ash, C. E., Geibel, J. F., Hagenson, R. L. and Soules, D. A. U.S. Patent 5,334,701 to Phillips Petroleum Company (August 2, 1994)
31 Stein, R. S. *Rubber Chem. Technol.* 1976, **46**, 458
32 Wilkes, G. L. 'Encyclopedia of Polymer Science and Engineering', 2nd edn, Vol. 14, Wiley Interscience, 1988, p. 542
33 J. Janzen, Personal communication
34 Hermans P. H. and Weidinger, A. *Text. Res. J.* 1961, **31**, 558
35 Muellerleile, J. T., Risch, B. G., Rodrigues, D. E., Wilkes, G. L. and Jones, D. M. *Polymer* 1993, **34**, 789
36 Risch, B. G., Wilkes, G. L. and Warakomski, J. M. *Polymer* 1993, **34**, 2330
37 Avrami, M. *J. Chem. Phys.* 1939, **7**, 1103; *J. Chem. Phys.* 1940, **8**, 212; *J. Chem. Phys.* 1941, **9**, 177
38 van Krevelen, D. W. *Chimia* 1978, **32**, 279
39 Wunderlich, B. 'Macromolecular Physics, Crystal Nucleation, Growth, Annealing', Vol. 2, Academic Press, New York, 1976
40 Hoffman, J. D. and Weeks, J. J. *J. Res. Natl. Bur. Stand. (A)* 1962, **66**, 13
41 Chung, J. S. and Cebe, P. *Polymer* 1992, **33**, 2312
42 Chung, J. S. and Cebe, P. *Polymer* 1992, **33**, 2325
43 Eisenberg, A. and Cayrol, B. *J. Polym. Sci: Part C* 1971, **35**, 129